ETAS: Zero-Shot Transformer Architecture Search via Network Trainability and Expressivity

Jiechao Yang[1,2] **Yong Liu**[1,2,*]
[1] Gaoling School of Artificial Intelligence, Renmin University of China, Beijing, China
[2] Beijing Key Laboratory of Big Data Management and Analysis Methods
{yangjiechao2021, liuyonggsai}@ruc.edu.cn

Abstract

Transformer Architecture Search (TAS) methods aim to automate searching for the optimal Transformer architecture configurations for a given task. However, they are impeded by the prohibitive cost of evaluating Transformer architectures. Recently, several Zero-Shot TAS methods have been proposed to mitigate this problem by utilizing zero-cost proxies to evaluate Transformer architectures without training. Unfortunately, they are limited to specific computer vision or natural language processing tasks. Nonetheless, most of them are developed based on empirical observations and lack theoretical guarantees. To solve this problem, we develop a new zero-cost proxy called NTSR that combines two theoretically-inspired indicators to measure the trainability and expressivity of Transformer networks separately. We then integrate it into an effective regularized evolution framework called ETAS to demonstrate its efficacy on various tasks. The results show that our proposed NTSR proxy can consistently achieve a higher correlation with the true performance of Transformer networks on both computer vision and natural language processing tasks. Further, it can significantly accelerate the search process for finding the best-performing Transformer architecture configurations.

1 Introduction

Transformer networks (Li et al., 2022a; Zhou et al., 2022; Chitty-Venkata et al., 2022) have attracted tremendous interest over recent years due to their effectiveness in learning long-range dependencies in data and superior performance across various tasks. They have gradually replaced traditional neural networks, such as Convolutional Neural Networks (CNNs) and Recurrent Neural Networks (RNNs), in a variety of domains including Natural Language Processing (NLP) (Javaheripi et al., 2022), Computer Vision (CV) (Chen et al., 2022), speech signal processing (Chitty-Venkata et al., 2022), and healthcare (Chitty-Venkata et al., 2022). Recently, the Transformer architecture has become the de facto backbone for most large language models (LLMs) (Zhao et al., 2023; Tornede et al., 2024). In real applications, it is often necessary to adjust the Transformer architecture configurations according to the specific tasks (Javaheripi et al., 2022), such as the depth of the network, the number of attention heads, embedding dimension, and the inner dimension of the feed-forward layer. However, manually tuning these parameters requires repeated refinement with expert experience, which is time-consuming and computationally expensive.

To solve this problem, various Transformer Architecture Search (TAS) methods (Lin et al., 2021; Chitty-Venkata et al., 2022; Wei et al., 2024; Chen et al., 2023) have been proposed, which automate the search for the optimal Transformer architecture configurations for a given task and data. The current popular TAS methods include reinforcement learning (Zhu et al., 2021), evolutionary search (Real et al., 2019; Zhou et al., 2024), one-shot (Li et al., 2021; Chen et al., 2021b), and predictor-based search (Wei et al., 2023; Ning et al., 2023). However, during the search process, they still demand a high computational cost to evaluate several hundred or thousands of architectures. Training a Transformer network can take hours or even days, thus hindering the practical application of TAS (Wei et al., 2024). Recently, zero-shot Neural Architecture Search (NAS) methods (Li et al., 2024) have attracted much attention as they design zero-cost proxies to estimate the performance of a network at the initialization stage. They can quickly evaluate the performance of a network in a few seconds by computing statistics from a single forward/backward propagation pass of the network with a minibatch of data at initialization (Abdelfattah et al., 2021). Nevertheless, Zhou et al. (2022) have shown the majority of existing zero-cost prox-

* Corresponding Author

ies are specifically designed for the CNN search spaces (e.g.,NAS-Bench-101 (Ying et al., 2019), NAS-Bench-201 (Dong and Yang, 2020), NAS-Bench-301 (Zela et al., 2022), TransNAS-Bench-101 (Duan et al., 2021)) and perform worse on the Transformer search space. They leverage the characteristics of Transformer networks and design a DSS zero-cost proxy that estimates synaptic diversity of multi-head self-attention (MSA) and synaptic saliency of the multilayer perceptron (MLP) in the Transformer network to rank its performance in a Vision Transformer (ViT) search space. Later, Chen et al. (2022) introduce a zero-cost proxy that measures the complexity of manifold propagation through ViT to estimate how complex a function can be approximated by a Vision Transformer network. Javaheripi et al. (2022) choose the number of decoder parameters in auto-regressive Transformers as a zero-cost proxy for the perplexity of the language model without the need for any model training.

Unfortunately, current zero-cost proxies for Transformer architectures are specifically designed for certain computer vision or natural language processing tasks. For example, existing zero-cost proxies for Transformers like DSS (Zhou et al., 2022) and TVT (Wei et al., 2023) are specially designed for Vision Transformer (ViT) encoder-only architectures. They show great performance on multiple vision tasks, but they perform relatively worse on the most used GPT auto-regressive architecture in NLP applications (Chen et al., 2022). On the other hand, LTS (Chen et al., 2022) show that decoder parameters serve as a good proxy for the performance of GPT-2 architectures on multiple NLP tasks. However, they perform relatively worse in ViT architecture (Zhou et al., 2024; Zhou and Zhu, 2024) as there exists a large amount of parameter redundancy in these structures, leading to over-parameterized networks that are prone to overfitting on small-scale datasets. Nonetheless, most of them are designed based on empirical observations and lack theoretical assurances. Can we design a theoretically-inspired zero-cost proxy applicable to multiple vision and language tasks? To this end, we propose a novel zero-cost proxy called NTSR that combines two theoretically-inspired indicators to measure the trainability and expressivity of Transformer networks. In particular, based on the theoretical underpinnings of deep neural network training, we design the NTKT metric that utilizes the trace of the mean Neural Tangent Kernel (NTK) to quantify the trainability of Transformer networks. Meanwhile, we design another SEPT metric that utilizes the upper bound of separation rank induced by the Transformer network to measure the capacity of Transformer networks to represent input dependencies. To demonstrate the effectiveness of our proposed NTSR zero-cost proxy for Transformer networks, we compare it to other popular zero-cost proxies in multiple search spaces. The results show that NTSR can consistently achieve a higher correlation with the true performance of Transformer networks on both computer vision and natural language processing tasks. To investigate the ability of our proposed NTSR zero-cost proxy to accelerate searching for the best-performing Transformer network, we further integrate it into an effective regularized evolution framework called ETAS. The results show that NTSR can significantly speed up finding the best-performing Transformer network.

2 Related Work

Transformer Architecture Search. The goal of Transformer Architecture Search (TAS) is to search for the best-performing Transformer configurations in an automated way for a given task. Recently, various TAS methods (Li et al., 2022b; Chitty-Venkata et al., 2022; Ye et al., 2024) have been proposed. One of the most popular methods is evolution-based Transformer architecture search (So et al., 2019, 2021; Su et al., 2022). They use an evolutionary search algorithm to find the optimal Transformer architecture within a given target budget. Another classic method is reinforcement learning (Zhu et al., 2021; Zhu, 2021), which uses a controller to sample high-quality Transformer architectures and updates the controller using the network's performance as a reward. However, current evolutionary search and reinforcement learning approaches need to collect a substantial number of network samples to train, which is costly and time-consuming. To reduce the search cost of TAS, one-shot methods (Chen et al., 2021a,b; Li et al., 2022a; Wang et al., 2023) have been proposed. They only train a huge supernetwork and obtain the performance of the sampled subnetwork through weight sharing. Nevertheless, training a huge supernetwork is non-trivial, and the memory consumption of a Transformer supernetwork increases with hidden size and runs out even with small values (Chitty-Venkata et al., 2022). Predictor-based methods (White et al., 2021; Shen et al., 2023) train

a surrogate model using a certain number of Transformer architecture-accuracy pairs and then use it to estimate the performance of unseen networks. Overall, the current popular TAS methods still need fully training massive architectures to find the optimal network, which demands a high computational cost. This highlights the great potential of developing zero-shot methods to replace the expensive training process in NAS with zero-cost proxies.

Zero-Cost Proxies. In recent years, various types of zero-cost proxies (Krishnakumar et al., 2022a; Li et al., 2024; Lee and Ham, 2024) have been proposed to rank the performance of networks at the initialization stage. One type consists of parametric saliency-based zero-cost proxies (White et al., 2022). They score the whole network by summing the changes in the saliency metric when a specific parameter of the network is removed. Abdelfattah et al. (2021) adopt several pruning-at-initialization metrics, including snip, grasp, synflow, and fisher, as parameter-level saliency-based zero-cost proxies for the network performance with a minibatch of data at initialization. Another type is network expressivity-based zero-cost proxies (Tu et al., 2022). They estimate the network performance by the expressivity of the network. Mellor et al. (2021) develop a heuristic NASWOT metric that utilizes the correlation of network activations between different data at initialization. Meanwhile, Chen et al. (2021c) select the number of linear activated regions represented by the network to measure the expressivity of a network. Additionally, there exists a type of zero-cost proxies inspired by deep learning theory (Zhou and Zhu, 2024; Shu et al., 2022b). Chen et al. (2021c) choose the condition number of Neural Tangent Kernel (NTK) to measure the trainability of networks and show it is negatively correlated with network performance. Later, Shu et al. (2022a) develop a label-agnostic and data-agnostic NASI metric that leverages the trace of NTK as an indicator for network performance. More recently, Li et al. (2023) found that the mean value and standard deviation of gradients across different samples affect the training convergence of networks. Based on the generalization theory of deep neural networks, they propose a theoretically-inspired zero-cost proxy called ZiCo that considers both the mean value and standard deviation of gradients in each layer of the network. Meanwhile, Jiang et al. (2023) use the minimum eigenvalue of the Pearson correlation matrix upon each layer of the feature maps to indicate the convergence of the network.

However, most of the existing zero-cost proxies are specially designed for CNN networks, whose internal architecture is distinctly different from the Transformer network. Zhou and Zhu (2024) have shown that the current zero-cost proxies for CNN cannot generalize well to the Transformer search space. To adapt well for the Transformer network, we develop a novel zero-cost proxy called NTSR that combines two theoretically-inspired indicators for measuring the trainability and expressivity of the Transformer network.

3 Method

In the context of TAS, the goal of zero-cost proxy is to accurately estimate the ranking of a Transformer network's performance at initialization. In fact, a good neural network architecture should have good trainability (i.e., how fast a network can converge via a gradient descent algorithm) and high expressivity (i.e., how complex functions a network can represent) (Chitty-Venkata et al., 2022; Chen et al., 2021c). In Sections 3.1 and 3.2, we design two theoretically-inspired indicators to reflect the trainability and expressivity of Transformer networks, separately. We then propose the NTSR zero-cost proxy that combines these two important indicators to measure the trainability and expressivity of a given Transformer network, and integrate it into an evolutionary search framework called ETAS to find the best-performing Transformer network architecture in Section 3.3.

3.1 Trainability of Transformer Network

With the rapid development of deep learning theory on neural networks, Neural Tangent Kernel (NTK) has emerged as an effective tool for characterizing the training dynamics of infinitely wide (Jacot et al., 2021) or finite wide (Novak et al., 2022) deep networks. It solved a classic question of "*how does training of neural networks work so well despite being highly nonconvex?*" (Yang, 2020). Lee et al. (2019) have demonstrated that under the large width limit and constant NTK assumption, the predictions of a neural network evolving like a linear model throughout gradient descent training.

NTK of Transformer. Assume there exists a batch of M sequences with T tokens $\mathcal{X} = \{\boldsymbol{x}_{\alpha,1}, \cdots, \boldsymbol{x}_{\alpha,T}\}_{\alpha=1}^{M}$ and a standard depth-L Transformer network with one input embed-

ding layer and L transformer blocks. The output of Transformer network at the L-th block is $\{\boldsymbol{z}_{\alpha,1}^L, \cdots, \boldsymbol{z}_{\alpha,T}^L\}_{\alpha=1}^M$. After that, we define the NTK of a Transformer network $\mathbf{K}(\mathcal{X},\mathcal{X}) \in \mathbb{R}^{Md_z^L \times T \times Md_z^L \times T}$, each element of the 4-dimensional NTK tensor is:

$$\mathbf{K}_{\alpha_1,t_1,\alpha_2,t_2} = \nabla_{\boldsymbol{w}} \boldsymbol{z}_{\alpha_1,t_1}^L \left(\nabla_{\boldsymbol{w}} \boldsymbol{z}_{\alpha_2,t_2}^L\right)^{\mathsf{T}}, \quad (1)$$

where $\alpha_1, \alpha_2 \in \mathcal{X}$ are pairs of inputs sampled from training batch $\mathcal{X}$. $t_1, t_2 \in [T]$ is the token index.

Theorem 3.1 (Yang (2020))**.** *Let f be a neural network of standard architecture with scalar output and randomly initialized weights $\omega \sim \mathcal{N}\left(0, \sigma_\omega^2\right)$. If it satisfies Condition 1 in Yang (2020) and its nonlinearities have polynomially bounded weak derivatives, then its NTK Θ converges almost surely, over any finite set of inputs, to a deterministic kernel Θ_0, i.e., $\Theta \xrightarrow{a.s.} \Theta_0$ as its widths go to infinity.*

This theorem indicates the NTK of a standard Transformer network at initialization $\mathbf{K}(\mathcal{X},\mathcal{X})$ has a well-defined infinite-width limit. We can use it to predict the training convergence of the network. As shown in Equation (14), we can estimate the training convergence of the network through NTK at initialization. If $\boldsymbol{\Theta}_0$ can be represented through its eigenvectors and corresponding eigenvalues λ_i, then it can be inferred that the eigenvectors of $\boldsymbol{\Theta}_0$ coincide with those of $e^{-\eta\boldsymbol{\Theta}_0 t}$ with a transformation of eigenvalues $e^{-\eta\lambda_i t}$. This observation reveals that the network's convergence rate is intimately connected to eigenstructures of $\boldsymbol{\Theta}_0$. Consequently, a network with a NTK characterized by a greater total sum of eigenvalues, $i.e.$, $\sum_i \lambda_i$, is likely to achieve faster convergence and a lower loss.

However, directly computing $\sum_i \lambda_i$ of the 4-dimensional NTK tensor $\mathbf{K}(\mathcal{X},\mathcal{X})$ of a Transformer network is extremely challenging. This difficulty arises due to the dynamic nature of the network connections in Transformers, where the output at each token index focuses on different parts of the input sequence, as shown in Equation (7), resulting in distinct outputs for each token index. To solve this problem, we take the mean of the NTK tensor $\mathbf{K}(\mathcal{X},\mathcal{X})$ over the token indexes, which is defined as $\bar{\mathbf{K}}(\mathcal{X},\mathcal{X}) \in \mathbb{R}^{Md_z^L \times Md_z^L}$, where each element is:

$$\bar{\mathbf{K}}_{\alpha_1,\alpha_2} = \frac{1}{T^2} \sum_{t_1=1}^{T} \sum_{t_2=1}^{T} \nabla_{\boldsymbol{w}} \boldsymbol{z}_{\alpha_1,t_1}^L \left(\nabla_{\boldsymbol{w}} \boldsymbol{z}_{\alpha_2,t_2}^L\right)^{\mathsf{T}}. \quad (2)$$

Through the above operation, the four-dimensional NTK tensor $\mathbf{K}(\mathcal{X},\mathcal{X})$ is reduced to a standard two-dimensional matrix $\bar{\mathbf{K}}_{\alpha_1,\alpha_2}$. Besides, the matrix is symmetric and positive semi-definite, and the sum of eigenvalues is equivalent to the trace of $\bar{\mathbf{K}}(\mathcal{X},\mathcal{X})$. Calculating the trace of a matrix offers computational efficiency, effectively bypassing the complexities involved in eigenvalue determination. Consequently, we use the trace of $\bar{\mathbf{K}}_{\alpha_1,\alpha_2}$ as an indicator called NTKT for the training convergence of the network, which is defined as:

$$\begin{aligned} \mathrm{NTKT}(\boldsymbol{f}) &= \left\|\bar{\mathbf{K}}(\mathcal{X},\mathcal{X})\right\|_{\mathrm{tr}} = \sum_{i=1}^{M} \left\|\bar{\mathbf{K}}_{\alpha_i,\alpha_i}\right\|_{\mathrm{tr}} \\ &= \frac{1}{T^2} \sum_{\alpha_i=1}^{M} \sum_{t_i=1}^{T} \sum_{j=1}^{d_z^L} \left\|\nabla_{\boldsymbol{w}} z_{\alpha_i,t_i,j}^L\right\|_2^2. \end{aligned} \quad (3)$$

Theorem 3.2. *Assume a standard Transformer net $\boldsymbol{f}$ with randomly initialized weights $\omega \sim \mathcal{N}\left(0, \sigma_\omega^2\right)$. Under vanilla stochastic gradient descent (SGD) optimizer and the first-order Taylor expansion, the mean of outputs over tokens at time step $s+1$ satisfies: $\bar{\boldsymbol{f}}_{s+1}(\mathcal{X}) - \bar{\boldsymbol{f}}_s(\mathcal{X}) = -\eta_s \bar{\mathbf{K}}(\mathcal{X},\mathcal{X}) \mathcal{L}'\left(\bar{\boldsymbol{f}}_s(\mathcal{X})\right)$, where η_s is the learning rate at step s. Then, $\mathrm{NTKT}(\boldsymbol{f})$ is positively correlated with the convergence rate of network $\boldsymbol{f}$.*

The proof of this theorem can be found in Appendix A.2. This theorem shows that NTKT provides a reasonable estimate for the training convergence of the network. In general, a larger NTKT score indicates that the corresponding network will converge faster and learn more efficiently.

3.2 Expressivity of Transformer Network

The success of Transformer networks largely relies on attention mechanism to learn complex dependencies among input sequences for different tasks. Intuitively, the stronger a Transformer network can model dependencies between inputs, the greater its capability to represent input information. **Is there a quantitative metric to measure the expressivity of a Transformer network at initialization?** To solve this problem, we introduce separation rank as a metric to quantify its ability for modeling dependencies between inputs of a Transformer network.

Separation Rank for Transformer. As shown in Equation (15), the separation rank directly reflects the core attention mechanism in Transformer networks. The self-attention layer dynamically learns

to correlate any inter-dependent subsets of the inputs (Levine et al., 2020). When a transformer network learns more dependencies between inputs, the separation rank induced by this network will have a higher value. Levine et al. (2020) have demonstrated a tight bound on the separation rank of Transformer networks with respect to the dependence on depth and width. Further, they leverage this bound to determine the optimal depth-to-width ratio for a given Transformer network size.

Theorem 3.3 (Levine et al. (2020)). *Let $f^{i,t,L,d_x,H}$ be the i-th scalar output at the t token index of a standard depth-L Transformer net $\boldsymbol{f}$ with dimension d_x and the number of heads H per layer. Then, its separation rank $w.r.t.$ balanced partitions, which obey $A \cup B = [T], |A| = |B| = T/2$, is invariant to identity of the partition, i.e., $A \cup B = [T], \tilde{A} \cup \tilde{B} = [T]$, such that $|A|, |B|, |\tilde{A}|, |\tilde{B}| = T/2$:* $\mathrm{sep}_{(A,B)}(f^{i,t,L,d_x,H}) = \mathrm{sep}_{(\tilde{A},\tilde{B})}(f^{i,t,L,d_x,H})$.

This theorem reveals that the separation rank induced by the standard Transformer network remains consistent under different balanced partitions of inputs. Next, we will omit the specification of any balanced partition of inputs, denoting it as $\mathrm{sep}(f^{i,t,L,d_x,H})$. Wies et al. (2021) further demonstrate the existence of an embedding rank bottleneck in the expressivity of the Transformer network. They showed that $\log(\mathrm{sep}(f^{i,t,L,d_x,H})) = \tilde{O}\left(L \cdot \min\{r, d_x\}\right)$, where r is the embedding rank defined as $r = \mathrm{rank}(\boldsymbol{W}_V)$.

However, the current study mainly focuses on the separation rank of the Transformer network with the same dimension d_x per layer. In this study, we extend the separation rank to the Transformer network where each block l has different d_z^l and d_{in}^l dimensions. This makes it more difficult to analyze. To solve this problem, we follow the relaxations by Wies et al. (2021) and Levine et al. (2020). We put all the position-wise feed-forward layers at the end since the feed-forward operation does not mix different locations and learn the dependencies between inputs. We then remove all the normalization layers and omit the ReLU and softmax non-linearities. The reasons for doing this can be referred to in Wies et al. (2021) and Levine et al. (2020). Though these relaxations are shown to weaken the overall network performance, they are much less pertinent to the ability of the core self-attention mechanism to model dependencies between different places at the input. Consequently, the multi-head attention operation of each block l in Equation (8) can be simplified as:

$$f_t^{l+1} = \sum_{t'=1}^{T} \sum_{h=1}^{H} \left\langle \boldsymbol{W}^{q,l,h} f_t^l, \boldsymbol{W}^{k,l,h} f_{t'}^l \right\rangle \boldsymbol{W}^{o,l,h} \boldsymbol{W}^{v,l,h} f_{t'}^l. \tag{4}$$

By forward propagating the above operations layer-by-layer, we can obtain the upper bound on the separation rank of the Transformer network with different dimensions d_z^l per layer.

Theorem 3.4. *Let f_t^L be the output at the t token index of a standard depth-L Transformer net $\boldsymbol{f}$ with dimension d_z^l and the number of heads H per layer. Then, its separation rank $w.r.t.$ balanced partitions satisfies* $\log(\mathrm{sep}(f_t^L)) \leq \log(\sum_{l=1}^{L} d_z^l) + \log(\sum_{l=1}^{L} \frac{1-(d_z^l)^{T+1}}{1-d_z^l})$.

The proof of this theorem is shown in Appendix A.2. This theorem shows that the separation rank of the Transformer net $\boldsymbol{f}$ can be upper bounded by a constant, which is related to the depth of the network L, the number of tokens T, and the sum of dimensions $\sum_{l=1}^{L} d_z^l$. Thus, we use this bound to measure the amount of dependencies modeled by the Transformer net. We name this measure as SEPT, which is defined as:

$$\mathrm{SEPT}(\boldsymbol{f}) = \log(\sum_{l=1}^{L} d_z^l) + \log(\sum_{l=1}^{L} \frac{1-(d_z^l)^{T+1}}{1-d_z^l}) \tag{5}$$

SEPT measures the Transformer network's ability to model dependencies between different places of the input. In general, a larger SEPT score indicates that the corresponding Transformer network has a stronger expressivity regarding different dependencies between inputs.

3.3 Zero-Shot Transformer Architecture Search via Network Trainability and Expressivity

NTSR. How can we combine the two theoretically-inspired indicators, NTKT and SEPT, to find the best-performing Transformer network at initialization? To answer this question, we propose a new zero-cost proxy called NTSR to make a trade-off between the network's trainability and expressivity. Note that the magnitudes of NTKT and SEPT scores may differ significantly, and their ranges are unknown before computing on the whole search space. Hence, we cannot

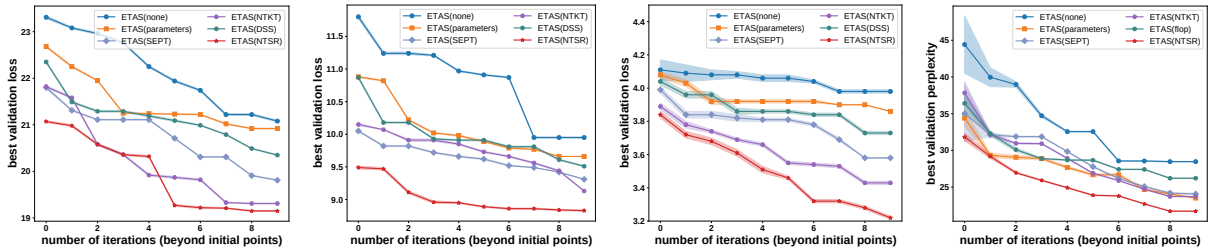

(a) (b) (c) (d)

Figure 1: The best-found valid loss over the number of iterations (beyond initial points) of various methods on (a) the ImageNet1k dataset of the Autoformer tiny search space, (b) the ImageNet1k dataset of the Autoformer small search space, (c) the ImageNet1k dataset of the Autoformer base search space, (d) the Wikitex103 dataset of the GPT-2 search space.

directly normalize NTKT and SEPT scores before searching the network. To avoid this problem, instead of using the numerical values of NTKT and SEPT, we combine the relative ranking of NTKT and SEPT by comparing the sampled set of architectures, which is defined as:

$$\mathrm{NTSR}(\boldsymbol{f}) = \frac{1}{2}(\mathrm{R}(\mathrm{NTKT}(\boldsymbol{f})) + \mathrm{R}(\mathrm{SEPT}(\boldsymbol{f}))), \tag{6}$$

where $\mathrm{R}(\mathrm{NTKT}(\boldsymbol{f}))$ and $\mathrm{R}(\mathrm{SEPT}(\boldsymbol{f}))$ represent the relative ranking of the network $\boldsymbol{f}$ converted from the $\mathrm{NTKT}(\boldsymbol{f})$ and $\mathrm{SEPT}(\boldsymbol{f})$ among the sampled set of architectures. In general, a higher rank of NTSR indicates that the network has better trainability and expressivity.

ETAS. As described above, our proposed NTSR zero-cost proxy provides a reasonable estimation of the network's performance. **The next major question is how to construct an efficient NAS framework on top of it?** To solve this problem, we integrate it into a popular regularized evolution framework called ETAS. We first randomly sample N_0 network architectures from the search space and then pick the top n_0 networks according the ranking of NTSR as the initial parent population to warmup the whore algorithm. Through warmup, we can find a better local initial population, thus potentially expediting the discovery of the optimal network. Note that the sample size N_0 is much larger than the number of networks we can afford to train. After that, we generate N_m candidate architectures by mutating the parent architectures at each iteration m and then select top n_m architectures from the current N_m candidate architectures according the ranking of NTSR. We then evaluate the selected architectures and update the parent population. The algorithm details of our proposed ETAS framework is given in the Appendix A.3.

4 Experiments and Discussion

In this section, we choose to search for the most popular Vision Transformer (ViT) and GPT-2 architectures in the computer vision and natural language processing domains, respectively. We compare our proposed NTSR zero-cost proxy with several zero-cost proxies for Transformers, including DSS (Zhou et al., 2022), Length Distortion (LD) (Chen et al., 2022), and conventional zero-cost proxies for CNNs like snip (Abdelfattah et al., 2020), grad_norm (White et al., 2022), NASWOT (Mellor et al., 2021), zico (Li et al., 2023), and MeCo (Jiang et al., 2023). Since Ning et al. (2021) have demonstrated that the number of flops and parameters serve as competitive proxies for network performance compared to most zero-cost proxies under the CNN search space, we also add them for comparison. To perform an ablation study on our proposed NTSR proxy, we include NTKT and SEPT alone as zero-cost proxies for comparison. Here, we choose the widely used Spearman's ρ (Krishnakumar et al., 2022b) and Kendall's τ (Ning et al., 2021) rank correlation metrics to evaluate their predictive ability.

4.1 Searching for ViT

To make a fair comparison, we employ the same search space of AutoFormer (Chen et al., 2021a), which searches the key components of the ViT architecture including embedding dimension, Q-K-V dimension, number of heads, MLP ratio, and network depth. It contains more than 1.7×10^{16} candidate architectures covering three common ranges of model size, *i.e.*, tiny (4-9 M), small (14-34 M),

Zero-cost proxies	tiny		small		base	
	KT	SPR	KT	SPR	KT	SPR
Autoformer (Chen et al., 2021a)	0.74	0.92	0.75	0.94	0.76	0.95
params	0.57±0.00	0.76±0.00	0.64±0.00	0.81±0.00	0.60±0.00	0.81±0.00
flops	0.49±0.00	0.68±0.00	0.58±0.00	0.78±0.00	0.52±0.00	0.74±0.00
snip	0.56±0.03	0.74±0.03	0.59±0.01	0.76±0.03	0.58±0.06	0.79±0.08
grad_norm	0.33±0.05	0.51±0.04	0.54±0.03	0.72±0.03	0.58±0.04	0.77±0.06
NASWOT	0.54±0.02	0.71±0.02	0.57±0.03	0.75±0.04	0.50±0.02	0.71±0.03
zico	0.48±0.03	0.65±0.03	0.43±0.02	0.62±0.03	0.43±0.04	0.62±0.05
MeCo	0.46±0.03	0.68±0.02	0.47±0.01	0.66±0.03	0.47±0.01	0.66±0.02
DSS	0.66±0.01	0.80±0.02	0.65±0.02	0.82±0.02	0.64±0.03	0.84±0.05
LD	0.52±0.02	0.69±0.02	0.60±0.03	0.81±0.04	0.59±0.03	0.80±0.03
SEPT	0.71±0.00	0.89±0.00	0.72±0.00	0.89±0.00	0.69±0.00	0.87±0.00
NTKT	0.70±0.02	0.87±0.02	0.70±0.03	0.86±0.02	0.72±0.02	0.90±0.02
NTSR	**0.74±0.01**	**0.90±0.02**	**0.74±0.02**	**0.91±0.02**	**0.75±0.01**	**0.92±0.01**

Table 1: The ranking correlation of different zero-cost proxies on the ImageNet-1k dataset of the AutoFormer search space over 5 independent runs with different random seeds, where KT and SPR represent Kendall's τ and Spearman's ρ rank correlation metrics, respectively.

Method	tiny			small			base		
	top1(%)	params(M)	flops(B)	top1(%)	params(M)	flops(B)	top1(%)	params(M)	flops(B)
ViT/16 (Dosovitskiy et al., 2021)	74.5	5.7	1.2	78.8	22.1	4.7	77.9	86	55.4
DeiT (Touvron et al., 2021)	72.2	5.7	1.2	79.9	22.1	4.7	81.8	86	17.5
ConViT (d'Ascoli et al., 2021)	73.1	6.0	1.0	81.3	27.0	5.4	82.4	86	17.0
Autoformer (Chen et al., 2021a)	74.7	5.9	1.3	81.7	22.9	4.9	82.4	54	11.0
PreNAS (Wang et al., 2023)	77.1	5.9	1.4	81.8	22.9	5.1	82.6	54	11.0
ETAS(none)	73.6	5.8	1.2	80.2	23.7	5.2	80.2	51	10.4
ETAS(parameters)	74.6	5.9	1.2	81.6	29.2	6.1	81.9	86	18.0
ETAS(SEPT)	77.2	5.9	1.2	82.3	27.6	5.8	82.4	54	11.2
ETAS(NTKT)	76.9	5.8	1.3	82.1	24.5	5.2	82.9	84	17.6
ETAS(DSS)	75.3	5.9	1.4	81.7	22.6	4.9	82.1	52	12.0
ETAS(NTSR)	**78.1**	5.9	1.4	**82.6**	28	5.9	**83.4**	82	15.5

Table 2: The test accuracy of various methods on the test set of the ImageNet-1k dataset, where ETAS(none) represents the ETAS without a zero-cost proxy.

Zero-cost proxies	CIFAR-100		flowers		chaoyang	
	KT	SPR	KT	SPR	KT	SPR
TVT (Wei et al., 2023)	0.66	0.78	0.73	0.82	0.25	0.39
params	0.41	0.53	0.46	0.63	-0.16	0.02
flops	0.39	0.47	0.43	0.56	-0.20	-0.04
snip	0.26	0.34	0.32	0.45	-0.03	0.12
grad_norm	0.42	0.55	0.47	0.59	0.14	0.36
NASWOT	0.59	0.73	0.66	0.78	0.21	0.45
zico	0.51	0.70	0.59	0.78	0.16	0.34
MeCo	0.60	0.74	0.62	0.78	0.20	0.41
DSS	0.49	0.63	0.54	0.71	0.17	0.32
LD	0.37	0.52	0.40	0.54	-0.12	0.03
SEPT	0.67	0.81	0.71	0.85	0.21	0.42
NTKT	0.69	0.84	0.74	0.89	0.27	0.49
NTSR	**0.71**	**0.86**	**0.78**	**0.90**	**0.30**	**0.51**

Table 3: The ranking correlation of different zero-cost proxies on three tiny datasets (CIFAR-100, Flowers, Chaoyang) of the AutoFormer search space, where KT and SPR represent Kendall's τ and Spearman's ρ rank correlation metrics, respectively.

Zero-cost proxies	WikiText103		LM1B	
	KT	SPR	KT	SPR
params	0.79±0.00	0.94±0.00	0.77±0.00	0.92±0.00
flops	0.65±0.00	0.80±0.00	0.51±0.00	0.72±0.00
snip	0.40±0.02	0.57±0.04	0.48±0.02	0.66±0.03
grad_norm	0.15±0.02	0.23±0.03	0.06±0.01	0.14±0.01
NASWOT	0.24±0.02	0.37±0.02	0.32±0.01	0.48±0.02
zico	0.18±0.01	0.36±0.02	0.15±0.01	0.26±0.02
MeCo	0.49±0.02	0.65±0.02	0.42±0.01	0.61±0.01
DSS	0.26±0.02	0.35±0.02	0.24±0.01	0.32±0.01
LD	0.48±0.03	0.64±0.03	0.37±0.01	0.50±0.02
SEPT	0.78±0.00	0.94±0.00	0.79±0.00	0.95±0.00
NTKT	0.80±0.02	0.96±0.02	0.78±0.01	0.92±0.02
NTSR	0.81±0.01	0.98±0.01	0.80±0.01	0.96±0.01

Table 4: The ranking correlation of different zero-cost proxies on the WikiText103 and LM1B datasets of GPT-2 search space over 5 independent runs with different random seeds, where KT and SPR represent Kendall's τ and Spearman's ρ rank correlation metrics, respectively.

and base (42-75 M). We randomly sample 1000 networks for each network setup since it is computationally infeasible to evaluate all networks of the large AutoFormer search space. After that, we compute the rank correlation between these zero-cost proxy scores and the true accuracy of these sampled networks on the ImageNet-1K dataset. Table 1 shows the performance of various zero-cost proxies across three setups, *i.e.*, tiny, small, and base. The results show that our proposed NTSR proxy can achieve similar ranking correlation with the one-shot AutoFormer method and perform better than other zero-cost proxies.

To demonstrate the effect of the NTSR proxy on accelerating TAS, we integrate it into the ETAS framework. Here, we choose to incorporate the top-5 zero-cost proxies from Table 1 into our proposed ETAS framework to evaluate their performance on speeding up the regularized evolution algorithm in discovering the best ViT architecture. The implementation details and experimental settings of these methods are summarized in Appendix A.4.1. Figures 1(a) to 1(c) show the best-found valid loss over number of iterations of various methods. The test loss of various methods on the test set of ImageNet-1k dataset is shown in Table 2. The results reveal that our proposed NTSR zero-cost proxy can achieve higher rank correlation across three setups. It can find a Transformer network architecture with lower validation loss using fewer iterations.

To further demonstrate the flexibility of our proposed NTSR proxy, we compare it with the recently proposed TVT (Wei et al., 2023) zero-cost proxy for ViT on three tiny datasets (CIFAR-100, Flowers, Chaoyang) of the AutoFormer search space.

Methods	valid perplexity (PPL)	latency(ms)	CO2 (lbs)	perplexity/latency MAPD (%)
LTS (Javaheripi et al., 2022)	23.68	17	0.02	0.6
GPT-2 (117M) (Radford et al., 2019)	29.41	18	-	-
GPT-2 (345M) (Radford et al., 2019)	22.76	24	-	-
ETAS(none)	28.47±0.04	20	0.01	1.6
ETAS(parameters)	23.51±0.05	23	0.03	0.8
ETAS(flop)	26.21±0.05	22	0.05	0.7
ETAS (SEPT)	24.07±0.03	20	0.04	0.7
ETAS (NTKT)	23.72±0.04	18	0.04	0.6
ETAS(NTSR)	**21.72±0.03**	19	0.04	0.5

Table 5: The validation perplexity of different methods on the WikiText103 dataset of the GPT-2 search space over 5 independent runs with different random seeds.

Here, we randomly sample 100 ViT architectures from the AutoFormer search space and compute the Kendall ranking correlation and Spearman ranking correlation between distillation accuracy and different zero-cost proxies. The results reveal that our proposed NTSR zero-cost proxy still performs better on these three tiny datasets.

4.2 Searching for GPT-2

The GPT-2 search space used in this section is largely based on the design of the LTS (Javaheripi et al., 2022) search space on the WikiText-103 (Merity et al., 2017) and One Billion Word (LM1B) (Chelba et al., 2014) datasets. It consists of the number of layers ($n\_layer \in \{2, \ldots, 16\}|1$), number of attention heads ($n\_head \in \{2, 4, 8\}$), decoder output dimension for each layer ($d\_model \in \{128, \ldots, 1024\}|64$), inner dimension of the feed forward network for each layer ($d\_inner \in \{256, \ldots, 4096\}|64$), and embedding dimension ($d\_embed \in \{128, 256, 512\}$). Unlike the LTS search space, we fix the adaptive input embedding factor to $k = 4$ to approximate the standard Transformer network with non-adaptive input embedding. We add a constraint that d_inner must be larger than $2d\_model$ to avoid training collapse of the network. To quantify the distance between the proxy and ground truth Pareto front, we use the mean average perplexity difference (MAPD) metric used in LTS, which is defined as: $d_{avg} = \frac{1}{N}\sum_{i=1}^{N}\frac{|p_i - p_{gt,i}|}{p_{gt,i}}$, where p_i denotes the i-th point on the proxy Pareto front and $p_{gt,i}$ is the closest ground truth Pareto front to p_i.

For each dataset, we randomly sample 500 networks and compute zero-cost proxies for each network. We train each GPT-2 model from scratch to obtain its true validation perplexity. After that, we compute rank correlation between these proxy scores and true validation perplexity of these sampled networks on the WikiText-103 and One Billion Word datasets. Table 4 shows the performance of various zero-cost proxies. To demonstrate the effect

of the NTSR proxy on speeding up TAS, we integrate it into the ETAS framework. Here, we choose to incorporate the top-5 zero-cost proxies from Table 4 into our proposed ETAS framework to evaluate their impact on speeding up the regularized evolution algorithm in discovering the best GPT-2 architecture on the WikiText-103 dataset. The implementation details and experimental settings of these methods are summarized in Section 4.2.

The validation perplexity of various methods on GPT-2 search space is shown in Table 5. The results reveal that our proposed NTSR proxy has a higher rank correlation with the true validation perplexity. It can significantly speed up finding better-performing Transformer network architectures with fewer iterations. In contrast, the zero-cost proxies for Transformers like DSS and LD perform worse on this GPT-2 search space. This may be because they are specially designed for the ViT transformer architecture and thus generalize worse on the GPT Transformer network. Furthermore, our proposed NTSR proxy is closer to the true Pareto front compared to other zero-cost proxies.

4.3 Ablation Studies

As shown above, for some tasks like the WikiText-103 dataset within the GPT-2 search space (see Table 4), NTKT performs better than SEPT and achieves lower validation perplexity. However, for certain tasks like the ImageNet-1k dataset within the AutoFormer small search space (see Table 1), SEPT performs better than NTKT. Our proposed NTSR zero-cost proxy combines the two theoretically-inspired indicators, NTKT and SEPT, and obtains consistently better performance across multiple tasks. To further analyze the combination effect of these two indicators, we perform ablation experiments on the combination coefficients of NTKT and SEPT (Equation (6)) on the WikiText-103 dataset within GPT-2 search space and the ImageNet-1k dataset within the AutoFormer small search space. The results are shown in Section 4.3. The results demonstrate the advantage of combining NTKT and SEPT indicators equally. This may be because combining NTKT and SEPT equally allows them to complement each other.

5 Limitation and Conclusion

In this study, we propose a novel zero-cost proxy for Transformer networks called NTSR to evaluate the performance of Transformers at initialization. Compared to other popular zero-cost proxies for Transformer networks, our proposed proxy is designed based on deep neural network learning theory in terms of the trainability and expressivity of Transformer networks. It achieves better performance on both NLP and CV tasks. However, our proposed method is limited to decoder-only Transformer architectures. In the future, we hope our proposed proxy can extend to other complex types of Transformer networks like BERT (Devlin et al., 2019) and T5 (Raffel et al., 2020).

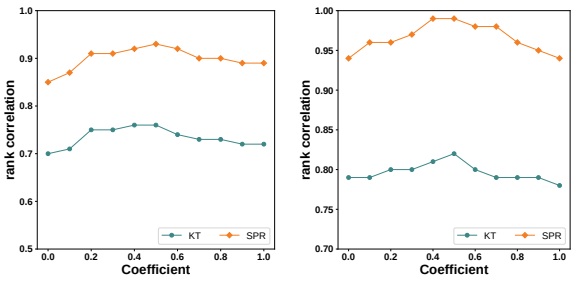

(a) (b)

Figure 2: The ranking correlation of different combination coefficients of NTKT and SEPT on the (a) ImageNet-1k dataset within the AutoFormer small search space and (b) WikiText-103 dataset within the GPT-2 search space, where KT and SPR represent Kendall's τ and Spearman's ρ rank correlation metrics, respectively.

Acknowledgements

We thank the anonymous reviewers for their valuable and constructive suggestions and comments. This work is supported by the Beijing Natural Science Foundation (No.4222029); the National Natural Science Foundation of China (N0.62076234); the National Key Research and Development Project (No.2022YFB2703102); the "Intel ligent Social Governance Interdisciplinary Platform, Ma jor Innovation & Planning Interdisciplinary Platform for the "Double-First Class" Initiative, Renmin University of China"; the Beijing Outstanding Young Scientist Program (NO.BJJWZYJH012019100020098); the Public Computing Cloud, Renmin University of China; the Fundamental Research Funds for the Central Universities, and the Research Funds of Renmin University of China (NO.2021030199), the Huawei-Renmin University joint program on Informa tion Retrieval: the Unicom Innovation Ecological Coopera tion Plan; the CCF-Huawei Populus Grove Fund.

References

Mohamed S Abdelfattah, Abhinav Mehrotra, Łukasz Dudziak, and Nicholas Donald Lane. 2020. Zero-cost proxies for lightweight nas. In *ICLR*.

Mohamed S. Abdelfattah, Abhinav Mehrotra, Lukasz Dudziak, and Nicholas Donald Lane. 2021. Zero-cost proxies for lightweight NAS. In *ICLR*.

Sanjeev Arora, Simon Du, Wei Hu, Zhiyuan Li, and Ruosong Wang. 2019. Fine-grained analysis of optimization and generalization for overparameterized two-layer neural networks. In *ICML*, pages 322–332.

Gregory Beylkin and Martin J Mohlenkamp. 2002. Numerical operator calculus in higher dimensions. In *PNAS*, 16, pages 10246–10251.

Ciprian Chelba, Tomás Mikolov, Mike Schuster, Qi Ge, Thorsten Brants, Phillipp Koehn, and Tony Robinson. 2014. One billion word benchmark for measuring progress in statistical language modeling. In *INTERSPEECH*, pages 2635–2639.

Minghao Chen, Houwen Peng, Jianlong Fu, and Haibin Ling. 2021a. Autoformer: Searching transformers for visual recognition. In *ICCV*, pages 12250–12260.

Shiming Chen, Ziming Hong, Wenjing Hou, Guo-Sen Xie, Yibing Song, Jian Zhao, Xinge You, Shuicheng Yan, and Ling Shao. 2023. Transzero++: Cross attribute-guided transformer for zero-shot learning. *IEEE Trans. Pattern Anal. Mach. Intell.*, 45(11):12844–12861.

Tianyi Chen, Bo Ji, Tianyu Ding, Biyi Fang, Guanyi Wang, Zhihui Zhu, Luming Liang, Yixin Shi, Sheng Yi, and Xiao Tu. 2021b. Only train once: A one-shot neural network training and pruning framework. In *NeurIPS*, pages 19637–19651.

Wuyang Chen, Xinyu Gong, and Zhangyang Wang. 2021c. Neural architecture search on imagenet in four GPU hours: A theoretically inspired perspective. In *ICLR*.

Wuyang Chen, Wei Huang, Xianzhi Du, Xiaodan Song, Zhangyang Wang, and Denny Zhou. 2022. Auto-scaling vision transformers without training. In *ICLR*.

Sambasiva Rao Chinnamsetty, Mike Espig, Boris N Khoromskij, Wolfgang Hackbusch, and Heinz-Jürgen Flad. 2007. Tensor product approximation with optimal rank in quantum chemistry. *The Journal of Chemical Physics*, 127(8).

Krishna Teja Chitty-Venkata, Murali Emani, Venkatram Vishwanath, and Arun K. Somani. 2022. Neural architecture search for transformers: A survey. *IEEE Access*, 10:108374–108412.

Nadav Cohen, Or Sharir, and Amnon Shashua. 2016. On the expressive power of deep learning: A tensor analysis. In *COLT*, pages 698–728.

Nadav Cohen and Amnon Shashua. 2017. Inductive bias of deep convolutional networks through pooling geometry. In *ICLR*.

Stéphane d'Ascoli, Hugo Touvron, Matthew L. Leavitt, Ari S. Morcos, Giulio Biroli, and Levent Sagun. 2021. Convit: Improving vision transformers with soft convolutional inductive biases. In *ICML*, pages 2286–2296.

Jacob Devlin, Ming-Wei Chang, Kenton Lee, and Kristina Toutanova. 2019. BERT: pre-training of deep bidirectional transformers for language understanding. In *NAACL*, pages 4171–4186.

Xuanyi Dong and Yi Yang. 2020. Nas-bench-201: Extending the scope of reproducible neural architecture search. In *ICLR*.

Alexey Dosovitskiy, Lucas Beyer, Alexander Kolesnikov, Dirk Weissenborn, Xiaohua Zhai, Thomas Unterthiner, Mostafa Dehghani, Matthias Minderer, Georg Heigold, Sylvain Gelly, Jakob Uszkoreit, and Neil Houlsby. 2021. An image is worth 16x16 words: Transformers for image recognition at scale. In *ICLR*.

Yawen Duan, Xin Chen, Hang Xu, Zewei Chen, Xiaodan Liang, Tong Zhang, and Zhenguo Li. 2021. Transnas-bench-101: Improving transferability and generalizability of cross-task neural architecture search. In *CVPR*, pages 5251–5260.

Mohsen Ghassemi, Zahra Shakeri, Waheed U. Bajwa, and Anand D. Sarwate. 2019. Sample complexity bounds for low-separation-rank dictionary learning. In *ISIT*, pages 2294–2298.

Arthur Jacot, Franck Gabriel, and Clément Hongler. 2021. Neural tangent kernel: convergence and generalization in neural networks. In *STOC*, page 6.

Mojan Javaheripi, Gustavo de Rosa, Subhabrata Mukherjee, Shital Shah, Tomasz Religa, Caio Cesar Teodoro Mendes, Sébastien Bubeck, Farinaz Koushanfar, and Debadeepta Dey. 2022. Litetransformersearch: Training-free neural architecture search for efficient language models. In *NeurIPS*.

Tangyu Jiang, Haodi Wang, and Rongfang Bie. 2023. Meco: Zero-shot NAS with one data and single forward pass via minimum eigenvalue of correlation. In *NeurIPS*.

Arjun Krishnakumar, Colin White, Arber Zela, Renbo Tu, Mahmoud Safari, and Frank Hutter. 2022a. Nasbench-suite-zero: Accelerating research on zero cost proxies. In *Advances in Neural Information Processing Systems*, pages 28037–28051.

Arjun Krishnakumar, Colin White, Arber Zela, Renbo Tu, Mahmoud Safari, and Frank Hutter. 2022b. NASbench-suite-zero: Accelerating research on zero cost proxies. In *NeurIPS*.

Jaehoon Lee, Lechao Xiao, Samuel S. Schoenholz, Yasaman Bahri, Roman Novak, Jascha Sohl-Dickstein, and Jeffrey Pennington. 2019. Wide neural networks of any depth evolve as linear models under gradient descent. In *NeurIPS*, pages 8570–8581.

Junghyup Lee and Bumsub Ham. 2024. Az-nas: Assembling zero-cost proxies for network architecture search. *arXiv preprint arXiv:2403.19232*.

Yoav Levine, Noam Wies, Or Sharir, Hofit Bata, and Amnon Shashua. 2020. Limits to depth efficiencies of self-attention. In *NeurIPS*.

Changlin Li, Tao Tang, Guangrun Wang, Jiefeng Peng, Bing Wang, Xiaodan Liang, and Xiaojun Chang. 2021. Bossnas: Exploring hybrid cnn-transformers with block-wisely self-supervised neural architecture search. In *ICCV*, pages 12261–12271.

Guihong Li, Duc Hoang, Kartikeya Bhardwaj, Ming Lin, Zhangyang Wang, and Radu Marculescu. 2024. Zero-shot neural architecture search: Challenges, solutions, and opportunities. *IEEE Transactions on Pattern Analysis and Machine Intelligence*, pages 1–19.

Guihong Li, Yuedong Yang, Kartikeya Bhardwaj, and Radu Marculescu. 2023. Zico: Zero-shot NAS via inverse coefficient of variation on gradients. In *ICLR*.

Yanyu Li, Geng Yuan, Yang Wen, Ju Hu, Georgios Evangelidis, Sergey Tulyakov, Yanzhi Wang, and Jian Ren. 2022a. Efficientformer: Vision transformers at mobilenet speed. In *NeurIPS*.

Yanyu Li, Geng Yuan, Yang Wen, Ju Hu, Georgios Evangelidis, Sergey Tulyakov, Yanzhi Wang, and Jian Ren. 2022b. Efficientformer: Vision transformers at mobilenet speed. In *NeurIPS*, pages 12934–12949.

Ming Lin, Pichao Wang, Zhenhong Sun, Hesen Chen, Xiuyu Sun, Qi Qian, Hao Li, and Rong Jin. 2021. Zen-nas: A zero-shot NAS for high-performance image recognition. In *ICCV*, pages 337–346.

Joe Mellor, Jack Turner, Amos J. Storkey, and Elliot J. Crowley. 2021. Neural architecture search without training. In *ICML*, pages 7588–7598.

Stephen Merity, Caiming Xiong, James Bradbury, and Richard Socher. 2017. Pointer sentinel mixture models. In *ICLR*.

Xuefei Ning, Changcheng Tang, Wenshuo Li, Zixuan Zhou, Shuang Liang, Huazhong Yang, and Yu Wang. 2021. Evaluating efficient performance estimators of neural architectures. In *NeurIPS*, pages 12265–12277.

Xuefei Ning, Yin Zheng, Zixuan Zhou, Tianchen Zhao, Huazhong Yang, and Yu Wang. 2023. A generic graph-based neural architecture encoding scheme with multifaceted information. *IEEE Transactions on Pattern Analysis and Machine Intelligence*, 45(7):7955–7969.

Roman Novak, Jascha Sohl-Dickstein, and Samuel S. Schoenholz. 2022. Fast finite width neural tangent kernel. In *ICML*, pages 17018–17044.

Alec Radford, Jeff Wu, Rewon Child, David Luan, Dario Amodei, and Ilya Sutskever. 2019. Language models are unsupervised multitask learners. *OpenAI blog*.

Colin Raffel, Noam Shazeer, Adam Roberts, Katherine Lee, Sharan Narang, Michael Matena, Yanqi Zhou, Wei Li, and Peter J. Liu. 2020. Exploring the limits of transfer learning with a unified text-to-text transformer. *JMLR*, 21:140:1–140:67.

Esteban Real, Alok Aggarwal, Yanping Huang, and Quoc V. Le. 2019. Regularized evolution for image classifier architecture search. In *AAAI*, pages 4780–4789.

Yu Shen, Yang Li, Jian Zheng, Wentao Zhang, Peng Yao, Jixiang Li, Sen Yang, Ji Liu, and Bin Cui. 2023. Proxybo: Accelerating neural architecture search via bayesian optimization with zero-cost proxies. In *AAAI*.

Yao Shu, Shaofeng Cai, Zhongxiang Dai, Beng Chin Ooi, and Bryan Kian Hsiang Low. 2022a. NASI: label- and data-agnostic neural architecture search at initialization. In *ICLR*.

Yao Shu, Zhongxiang Dai, Zhaoxuan Wu, and Bryan Kian Hsiang Low. 2022b. Unifying and boosting gradient-based training-free neural architecture search. In *NeurIPS*.

David R. So, Quoc V. Le, and Chen Liang. 2019. The evolved transformer. In *ICML*, pages 5877–5886.

David R. So, Wojciech Manke, Hanxiao Liu, Zihang Dai, Noam Shazeer, and Quoc V. Le. 2021. Searching for efficient transformers for language modeling. In *NeurIPS*, pages 6010–6022.

Xiu Su, Shan You, Jiyang Xie, Mingkai Zheng, Fei Wang, Chen Qian, Changshui Zhang, Xiao-Gang Wang, and Chang Xu. 2022. Vitas: Vision transformer architecture search. In *ECCV*, pages 139–157.

Alexander Tornede, Difan Deng, Theresa Eimer, Joseph Giovanelli, Aditya Mohan, Tim Ruhkopf, Sarah Segel, Daphne Theodorakopoulos, Tanja Tornede, Henning Wachsmuth, and Marius Lindauer. 2024. AutoML in the age of large language models: Current challenges, future opportunities and risks. *Transactions on Machine Learning Research*.

Hugo Touvron, Matthieu Cord, Matthijs Douze, Francisco Massa, Alexandre Sablayrolles, and Hervé Jégou. 2021. Training data-efficient image transformers & distillation through attention. In *ICML*, pages 10347–10357.

Renbo Tu, Nicholas Roberts, Mikhail Khodak, Junhong Shen, Frederic Sala, and Ameet Talwalkar. 2022. Nas-bench-360: Benchmarking neural architecture search on diverse tasks. In *NeurIPS*.

AbdoulAhad Validi. 2014. Low-rank separated representation surrogates of high-dimensional stochastic functions: Application in bayesian inference. *Journal of Computational Physics*, 260:37–53.

Haibin Wang, Ce Ge, Hesen Chen, and Xiuyu Sun. 2023. Prenas: Preferred one-shot learning towards efficient neural architecture search. In *ICML*, pages 35642–35654.

Zimian Wei, Peijie Dong, Zheng Hui, Anggeng Li, Lujun Li, Menglong Lu, Hengyue Pan, and Dongsheng Li. 2024. Auto-prox: Training-free vision transformer architecture search via automatic proxy discovery. In *AAAI*, pages 15814–15822.

Zimian Wei, Hengyue Pan, Lujun Li, Peijie Dong, Zhiliang Tian, Xin Niu, and Dongsheng Li. 2023. Tvt: Training-free vision transformer search on tiny datasets. *arXiv preprint arXiv:2311.14337*.

Colin White, Mikhail Khodak, Renbo Tu, Shital Shah, Sébastien Bubeck, and Debadeepta Dey. 2022. A deeper look at zero-cost proxies for lightweight nas. In *ICLR Blog Track*.

Colin White, Arber Zela, Robin Ru, Yang Liu, and Frank Hutter. 2021. How powerful are performance predictors in neural architecture search? In *Proc. Conf. Neural Informat. Process. Syst.*, pages 28454–28469.

Noam Wies, Yoav Levine, Daniel Jannai, and Amnon Shashua. 2021. Which transformer architecture fits my data? A vocabulary bottleneck in self-attention. In *ICML*, pages 11170–11181.

Greg Yang. 2020. Tensor programs ii: Neural tangent kernel for any architecture. *arXiv preprint arXiv:2006.14548*.

Hancheng Ye, Chong Yu, Peng Ye, Renqiu Xia, Yansong Tang, Jiwen Lu, Tao Chen, and Bo Zhang. 2024. Once for both: Single stage of importance and sparsity search for vision transformer compression. *arXiv preprint arXiv:2403.15835*.

Chris Ying, Aaron Klein, Eric Christiansen, Esteban Real, Kevin Murphy, and Frank Hutter. 2019. Nas-bench-101: Towards reproducible neural architecture search. In *ICML*, pages 7105–7114.

Yang You, Jing Li, Sashank J. Reddi, Jonathan Hseu, Sanjiv Kumar, Srinadh Bhojanapalli, Xiaodan Song, James Demmel, Kurt Keutzer, and Cho-Jui Hsieh. 2020. Large batch optimization for deep learning: Training BERT in 76 minutes. In *ICLR*.

Arber Zela, Julien Niklas Siems, Lucas Zimmer, Jovita Lukasik, Margret Keuper, and Frank Hutter. 2022. Surrogate nas benchmarks: Going beyond the limited search spaces of tabular nas benchmarks. In *ICLR*, pages 1–36.

Wayne Xin Zhao, Kun Zhou, Junyi Li, Tianyi Tang, Xiaolei Wang, Yupeng Hou, Yingqian Min, Beichen Zhang, Junjie Zhang, Zican Dong, Yifan Du, Chen Yang, Yushuo Chen, Zhipeng Chen, Jinhao Jiang, Ruiyang Ren, Yifan Li, Xinyu Tang, Zikang Liu, Peiyu Liu, Jian-Yun Nie, and Ji-Rong Wen. 2023. A survey of large language models. *arXiv preprint arXiv:2303.18223*.

Qinqin Zhou, Kekai Sheng, Xiawu Zheng, Ke Li, Xing Sun, Yonghong Tian, Jie Chen, and Rongrong Ji. 2022. Training-free transformer architecture search. In *CVPR*, pages 10884–10893.

Qinqin Zhou, Kekai Sheng, Xiawu Zheng, Ke Li, Yonghong Tian, Jie Chen, and Rongrong Ji. 2024. Training-free transformer architecture search with zero-cost proxy guided evolution. *IEEE Transactions on Pattern Analysis and Machine Intelligence*.

Qiqi Zhou and Yichen Zhu. 2024. When training-free nas meets vision transformers: A neural tangent kernel perspective. In *ICASSP*, pages 7405–7409.

Wei Zhu. 2021. Autorc: Improving BERT based relation classification models via architecture search. In *ACL*, pages 33–43.

Wei Zhu, Xiaoling Wang, Yuan Ni, and Guotong Xie. 2021. Autotrans: Automating transformer design via reinforced architecture search. In *NLPCC*, pages 169–182.

A Appendix

A.1 Background

A.1.1 Standard Transformer

Assume a standard depth-L Transformer network has one input embedding layer and L transformer blocks. The input of the Transformer network is a sequence of T tokens $\{\boldsymbol{x}_t \in [V]\}_{t=1}^{T}$, where V is the number of vocabulary tokens. The embedding

layer transforms the input sequence $\{\boldsymbol{x}_t \in [V]\}_{t=1}^{T}$ to T sequenced d_x^1-dimensional vectors $\boldsymbol{z}_t^1, t \in [T]$, which is defined as $\boldsymbol{z}_t^1 = \boldsymbol{W}_V \boldsymbol{x}_t + \boldsymbol{p}_t$, where $\boldsymbol{W}_V \in \mathbb{R}^{d_x^1 \times V}$ is the learned word-embedding matrix, and $\boldsymbol{p}_t$ is the positional embedding vector. After that, $\boldsymbol{z}_t^1$ is recursively transformed into T sequenced d_x^l-dimensional vectors $\boldsymbol{z}_t^l, t \in [T], l \in [L] := \{1, \ldots, L\}$ through L transformer blocks. Each transformer block consists of two sublayers, *i.e.*, a multi-head self-attention sublayer and a position-wise feed-forward sublayer. Each block operation is defined as:

$$\text{Attn}_t^{l,h} = \text{SM}\left\{\frac{1}{\sqrt{d_a}}\left\langle \boldsymbol{W}^{q,l,h}\boldsymbol{z}_t^l, \boldsymbol{W}^{k,l,h}\boldsymbol{z}_{t'}^l \right\rangle\right\}, \tag{7}$$

$$\boldsymbol{f}_{\text{MHSA}}^{l,t} = \sum_{t'=1}^{T}\sum_{h=1}^{H} \text{Attn}_t^{l,h}\boldsymbol{W}^{o,l,h}\boldsymbol{W}^{v,l,h}\boldsymbol{z}_{t'}^l, \tag{8}$$

$$\boldsymbol{f}_{\text{FFN}}^{l,t} = \boldsymbol{W}_{\text{FFN2}}^l\, \sigma(\boldsymbol{W}_{\text{FFN1}}^l\, \text{LN}(\boldsymbol{f}_{\text{MHSA}}^{l,t} + \boldsymbol{z}_t^l)), \tag{9}$$

$$\boldsymbol{z}_t^{l+1} = \text{LN}(\boldsymbol{f}_{\text{FFN}}^{l,t}), \tag{10}$$

where SM and LN represent the softmax and layer normalization operations, respectively. $\text{Attn}_t^{l,h}$ is the attention score matrix between the vector $\boldsymbol{z}_t^l$ at position $t \in [T]$ and other vectors $\boldsymbol{z}_{t'}^l$ at position $t' \in [T]$ in the l-th transformer block. $\boldsymbol{f}_{\text{MHSA}}^{l,t}$ and $\boldsymbol{f}_{\text{FFN}}^{l,t}$ are the outputs of the multi-head self-attention sublayer and the point-wise feed-forward sublayer in the l-th transformer block, respectively. $\boldsymbol{W}^{q,l,h}, \boldsymbol{W}^{k,l,h}, \boldsymbol{W}^{v,l,h} \in \mathbb{R}^{d_z^l \times d_a^l}$ represent the query, key, and value weight matrices, respectively. $\boldsymbol{W}^{o,l,h} \in \mathbb{R}^{d_a^l \times d_z^l}$ represents the aggregated weights across H heads. d_a^l is the dimension of the transformer block l, *i.e.*, the width of the entire block. H is the number of heads and the dimension of each head in the transformer block l is $d_a^l = d_z^l/H$. σ represents the ReLU activation function. $\boldsymbol{W}_{\text{FFN1}}^l \in \mathbb{R}^{d_z^l \times d_{\text{in}}^l}, \boldsymbol{W}_{\text{FFN2}}^l \in \mathbb{R}^{d_{\text{in}}^l \times d_z^l}$ represent the inner feed-forward weight matrices. d_{in}^l is the inner dimension of the feed-forward sublayer, which is usually set to $4d_z^l$. Unlike traditional transformer networks stacking blocks with fixed sizes, in this study, we allow each transformer block l to have different d_z^l and d_{in}^l dimensions, enhancing its flexibility across different tasks.

A.1.2 Neural Tangent Kernel (NTK)

Formally, assume a deep neural network f parameterized by $\mathbf{w}$ has D output dimensions. Let $(\mathcal{X}, \mathcal{Y})$ be the training samples, and $\mathcal{L}$ the loss function. The outputs of the network are $\mathbf{f}(\mathcal{X}, \mathbf{w}) \in \mathbb{R}^{ND}$, where N is the number of training samples. During gradient descent training, the evolution of parameters $\mathbf{w}_s$ and output $\mathbf{f}(\mathcal{X}, \mathbf{w}_s)$ at time step s can be expressed as follows:

$$\dot{\mathbf{w}}_s = -\eta \nabla_{\mathbf{w}} \mathbf{f}(\mathcal{X}, \mathbf{w}_s)^\intercal \nabla_{\mathbf{f}(\mathcal{X}, \mathbf{w}_s)} \mathcal{L}, \tag{11}$$

$$\begin{aligned}\dot{\mathbf{f}}(\mathcal{X}, \mathbf{w}_s) &= \nabla_{\mathbf{w}} \mathbf{f}(\mathcal{X}, \mathbf{w}_s)\dot{\mathbf{w}}_s \\ &= -\eta \nabla_{\mathbf{w}} \mathbf{f}(\mathcal{X}, \mathbf{w}_s)\mathbf{f}(\mathcal{X}, \mathbf{w}_s)^\intercal \nabla_{\mathbf{f}(\mathcal{X}, \mathbf{w}_s)} \mathcal{L} \\ &= -\eta \boldsymbol{\Theta}_s(\mathcal{X}, \mathcal{X}) \nabla_{\mathbf{f}(\mathcal{X}, \mathbf{w}_s)} \mathcal{L}, \end{aligned} \tag{12}$$

where $\boldsymbol{\Theta}_s(\mathcal{X}, \mathcal{X}) \in \mathbb{R}^{ND \times ND}$ is the Neural Tangent Kernel (NTK) at time step s, defined as:

$$\boldsymbol{\Theta}_s(\mathcal{X}, \mathcal{X}) = \nabla_{\mathbf{w}} \mathbf{f}(\mathcal{X}, \mathbf{w}_s) \nabla_{\mathbf{w}} \mathbf{f}(\mathcal{X}, \mathbf{w}_s)^\intercal. \tag{13}$$

The NTK exactly captures the training dynamics of the network. Especially for the infinite wide network, under the mean-squared loss and a constant NTK assumption, *i.e.*, $\boldsymbol{\Theta}_s(\mathcal{X}, \mathcal{X}) \equiv \boldsymbol{\Theta}_0(\mathcal{X}, \mathcal{X})$, Equation (12) has a closed-form solution:

$$\mathbf{f}\left(\mathcal{X}, \mathbf{w}_s\right) = \left(\mathbf{I} - e^{-\eta \boldsymbol{\Theta}_0 s}\right) \mathcal{Y} + e^{-\eta \boldsymbol{\Theta}_0 s} \mathbf{f}\left(\mathcal{X}, \mathbf{w}_0\right), \tag{14}$$

where $\mathbf{f}\left(\mathcal{X}, \mathbf{w}_s\right)$ represents the outputs of the network at time step s, $\mathbf{I}$ is the identity matrix, $\mathbf{f}\left(\mathcal{X}, \mathbf{w}_0\right)$ is the output of the network at initialization, and η is the learning rate. This implies that the output of the network is determined by the training samples $(\mathcal{X}, \mathcal{Y})$, the initial weights $\mathbf{w}_0$, and the initial NTK $\mathbf{f}\left(\mathcal{X}, \mathbf{w}_0\right)$. Through the NTK at initialization, we can estimate the training convergence of a network. Arora et al. (2019) have demonstrated that the training convergence speed is faster in the direction corresponding to the larger NTK eigenvalues of the network.

A.1.3 Separation Rank

Separation rank was first proposed by Beylkin and Mohlenkamp (2002) for high-dimensional numerical analysis, and then applied to various areas including machine learning (Ghassemi et al., 2019), chemistry (Chinnamsetty et al., 2007), and physics (Validi, 2014). Recently, it has been applied to measure the input dependencies modeled by deep convolutional and recurrent networks (Cohen and Shashua, 2017; Cohen et al., 2016). Let (A, B) be a partition of the input locations, *i.e.*, A and B are disjoint subsets of the input sequence $[T] := \{1, \ldots, T\}$ and $A \cup B = [T]$. The separation rank of a function $f(\mathbf{x}_1, \ldots, \mathbf{x}_T)$ with respect

to partition (A, B) is the minimal number of summands that together sum up to equal f, where each summand is multiplicatively separable with respect to the partition (A, B), *i.e.*, each summand is equal to a product of two functions — one that takes in only inputs from the subset $\{\mathbf{x}_i : i \in A\}$ and another that intakes only inputs from the other subset $\{\mathbf{x}_j : j \in B\}$. Formally, the separation rank of $f : \left(\mathbb{R}^{d_x}\right)^T \to \mathbb{R}$ with respect to the partition (A, B) is defined as:

$$\begin{aligned}\mathrm{sep}_{(A,B)}(f) := \min \Big\{ & R \in \mathbb{N} \cup \{0\} : \\ & \exists g_1^A, \ldots, g_R^A, g_1^B, \ldots, g_R^B : \left(\mathbb{R}^{d_x}\right)^{N/2} \to \mathbb{R}, \\ & f(\mathbf{x}_1, \ldots, \mathbf{x}_T) = \\ & \sum_{r=1}^{R} g_r^A\left(\{\mathbf{x}_i : i \in A\}\right) g_r^B\left(\{\mathbf{x}_j : j \in B\}\right) \Big\}.\end{aligned} \tag{15}$$

The separation rank quantifies the amount of input inter-dependency induced by the function $f(\mathbf{x}_1, \ldots, \mathbf{x}_T)$ with respect to partition (A, B). If the separation rank of a function $f(\mathbf{x}_1, \ldots, \mathbf{x}_T)$ with respect to partition (A, B) is 1, the function $f(\mathbf{x}_1, \ldots, \mathbf{x}_T)$ is multiplicatively separable with respect to partition (A, B), meaning that $\{\mathbf{x}_i : i \in A\}$ and $\{\mathbf{x}_j : j \in B\}$ are statistically independent. The larger $\mathrm{sep}_{(A,B)}(f)$ is, the more it models inter-dependency between $\{\mathbf{x}_i : i \in A\}$ and $\{\mathbf{x}_j : j \in B\}$. In other words, it means that the function $f(\mathbf{x}_1, \ldots, \mathbf{x}_T)$ can learn higher correlations between $\{\mathbf{x}_i : i \in A\}$ and $\{\mathbf{x}_j : j \in B\}$.

A.2 Proof

Proof of Theorem 3.2. Under the vanilla stochastic gradient descent (SGD) optimizer, the weight parameter is updated as follows:

$$\boldsymbol{w}_{s+1} = \boldsymbol{w}_s - \eta_s \frac{\partial \mathcal{L}}{\partial \boldsymbol{w}}\bigg|_{\boldsymbol{w}=\boldsymbol{w}_s} \tag{16}$$

Then, under the first-order Taylor expansion, the mean of output over tokens at time step $s+1$ satisfies:

$$\begin{aligned}\bar{\boldsymbol{f}}_{s+1}(\mathcal{X}) &= \bar{\boldsymbol{f}}_s(\mathcal{X}) - \eta_s\left(\frac{\partial \mathcal{L}}{\partial \boldsymbol{w}} \frac{\partial \bar{\boldsymbol{f}}_s(\mathcal{X})}{\partial \boldsymbol{w}}\right) \\ &= \bar{\boldsymbol{f}}_s(\mathcal{X}) - \eta_s \mathcal{L}'(\bar{\boldsymbol{f}}_s)\left(\frac{\partial \bar{\boldsymbol{f}}_s(\mathcal{X})}{\partial \boldsymbol{w}}\right)\left(\frac{\partial \bar{\boldsymbol{f}}_s(\mathcal{X})}{\partial \boldsymbol{w}}\right)^{\mathsf{T}} \\ &= \bar{\boldsymbol{f}}_s(\mathcal{X}) - \eta_s \mathcal{L}'(\bar{\boldsymbol{f}}_s)\bar{\mathbf{K}}(\mathcal{X}, \mathcal{X}).\end{aligned} \tag{17}$$

This reduces to a kernel gradient descent method. Thus, the convergence rate of the network is determined by the eigenstructure of the mean NTK $\bar{\mathbf{K}}(\mathcal{X}, \mathcal{X})$. If it can be diagonalized by eigenfunctions with corresponding eigenvalues λ_i, the sum of eigenvalues $\sum \lambda_i$ provides a upper bound for the convergence of the network. Since the mean NTK $\bar{\mathbf{K}}(\mathcal{X}, \mathcal{X})$ matrix is symmetric and symmetric. The trace of $\bar{\mathbf{K}}(\mathcal{X}, \mathcal{X})$ $i.e.$, NTKT is equal to the sum of eigenvalues $\sum \lambda_i$. Therefore, a larger NTKT score of the Transformer network indicates it converge faster. □

Proof of Theorem 3.4. According to the Equation (4), the output of each block l can be expressed as follows:

$$\boldsymbol{f}_t^{l+1} = \sum_{t'=1}^{T}\sum_{h=1}^{H}\left\langle \boldsymbol{W}^{q,l,h}\boldsymbol{f}_t^l, \boldsymbol{W}^{k,l,h}\boldsymbol{f}_{t'}^l \right\rangle \boldsymbol{W}^{o,l,h}\boldsymbol{W}^{v,l,h}\boldsymbol{f}_{t'}^l. \tag{18}$$

Let $\boldsymbol{M}^{l,h} = \boldsymbol{W}^{q,l,h}\boldsymbol{f}_t^l \boldsymbol{f}_t^{l^{\mathrm{T}}} \boldsymbol{W}^{k,l,h^{\mathrm{T}}}$, the Equation (4) can be expressed as:

$$\boldsymbol{f}_t^{l+1} = \sum_{t'=1}^{T}\sum_{h=1}^{H} \boldsymbol{W}^{o,l,h}\boldsymbol{M}^{l,h}\boldsymbol{W}^{v,l,h}\boldsymbol{f}_{t'}^l. \tag{19}$$

Assume there exits a balanced partition of the input locations (A, B), $i.e.$, each token index $P_t \in \{A, B\}$, A and B are disjoint subsets of input sequence $[T] := \{1, \ldots, T\}$ and $A \cup B = [T]$. The matrix multiplication in the $\boldsymbol{M}^{l,h}$ can be divided the sum over inputs indexed by A and B:

$$\begin{aligned}\boldsymbol{M}_{r_1,r_2}^{l,h} &= \sum_{t=1}^{T}[\boldsymbol{W}^{q,l,h}\boldsymbol{f}_t^l]_{r_1,t}[\boldsymbol{f}_t^{l^{\mathrm{T}}}\boldsymbol{W}^{k,l,h^{\mathrm{T}}}]_{t,r_2} \\ &= \sum_{t\in A}[\boldsymbol{W}^{q,l,h}\boldsymbol{f}_t^l]_{r_1,t}[\boldsymbol{f}_t^{l^{\mathrm{T}}}\boldsymbol{W}^{k,l,h^{\mathrm{T}}}]_{t,r_2} \\ &\quad + \sum_{t\in B}[\boldsymbol{W}^{q,l,h}\boldsymbol{f}_t^l]_{r_1,t}[\boldsymbol{f}_t^{l^{\mathrm{T}}}\boldsymbol{W}^{k,l,h^{\mathrm{T}}}]_{t,r_2}.\end{aligned} \tag{20}$$

Then the Equation (19) can be reformed as:

$$
\begin{aligned}
f_t^{l+1} &= \sum_{h\in[H]} \sum_{r_1,\ldots,r_T=1}^{d_a^l} \sum_{P_1,\ldots,P_T} \boldsymbol{W}^{o,l,h}\boldsymbol{W}^{v,l,h} f_t^l \\
&\quad \left(\prod_{t=1}^{T} [\boldsymbol{W}^{q,l,h} f_t^l]_{r_t,t} [{f_t^l}^{\mathrm{T}} \boldsymbol{W}^{k,l,h^{\mathrm{T}}}]_{t,r_t} \right) \\
&= \sum_{h\in[H]} \sum_{r_1,\ldots,r_T=1}^{d_a^l} \sum_{P_1,\ldots,P_T} \boldsymbol{W}^{o,l,h}\boldsymbol{W}^{v,l,h} f_t^l \\
&\quad \left(\sum_{t\in A} [\boldsymbol{W}^{q,l,h} f_t^l]_{r_t,t} [{f_t^l}^{\mathrm{T}} \boldsymbol{W}^{k,l,h^{\mathrm{T}}}]_{t,r_t} \right. \\
&\quad \left. \sum_{t\in B} [\boldsymbol{W}^{q,l,h} f_t^l]_{r_t,t} [{f_t^l}^{\mathrm{T}} \boldsymbol{W}^{k,l,h^{\mathrm{T}}}]_{t,r_t} \right) \\
&\leq \sum_{t=1}^{T} \sum_{r_1,\ldots,r_t=1}^{d_a^l} H \\
&= \sum_{t=1}^{T} (H d_a^l)^t = \sum_{t=1}^{T} (d_z^l)^t \\
&= d_z^l \frac{1-(d_z^l)^{T+1}}{1-d_z^l} \quad .
\end{aligned}
\tag{21}
$$

The separation rank at the l block satisfies:

$$
\log\left(\frac{\mathrm{sep}(f_t^{l+1})}{\mathrm{sep}(f_t^l)}\right) \leq \log(d_z^l) + \log\left(\frac{1-(d_z^l)^{T+1}}{1-d_z^l}\right) \tag{22}
$$

Then, the separation rank at the last block L satisfies:

$$
\log(\mathrm{sep}(f_t^L)) \leq \log\left(\sum_{l=1}^{L} d_z^l\right) + \log\left(\sum_{l=1}^{L} \frac{1-(d_z^l)^{T+1}}{1-d_z^l}\right) \tag{23}
$$

□

A.3 Algorithm Details of ETAS

To integrate our proposed NTSR zero-cost proxy into the ETAS framework, we first randomly sample N_0 networks from the Transformer search space and compute the relative rankings of these N_0 networks using NTSR. After that, we select the top n_0 network structures with the highest NTSR scores as the parent population and evaluate these networks to obtain their true performance. We add the network-performance pairs to the observed set. For each iteration m, we generate a pool of N_m candidate architectures by mutating the current parent population and select the top n_m architectures from N_m based on their NTSR scores. We then evaluate these n_m architectures and add their network-performance pairs to the current observed set. The parent population is updated by selecting the top n_0 networks from the current observed set. Finally, we select the top-performing architecture from the observed set. This process continues until the maximum number of iterations M is reached or the current best value has not improved for five successive iterations. The detailed algorithm of our proposed ETAS framework is summarized in Algorithm 1. Note that our proposed ETAS framework can also incorporate other zero-cost proxies.

Algorithm 1: ETAS

Input: Total number of iterations M, search space $\mathcal{A}$, parent population = $\oslash$, observed population = $\oslash$

Output: The best-performing architecture $\boldsymbol{f}^*$

Randomly sample N_0 networks from the search space $\mathcal{A}$;
Compute the relative ranking of N_0 initial networks by NTSR;
Select top n_0 networks as the parent population;
Evaluate n_0 networks and add the corresponding validation accuracy into the observed population;
for $m = 1$ ***to*** M **do**
    Generate N_m candidate architectures by mutating the network from the parent population;
    Compute the relative ranking of N_m initial networks by NTSR;
    Select the top n_m networks and evaluate them to obtain the corresponding validation accuracy;
    Add the n_m networks and their corresponding validation accuracy into the current observed set;
    Update the parent population by selecting the top n_0 networks from the current observed set;
end
return the best-performing architecture from the observed set.

A.4 Experimental settings

A.4.1 Experimental settings of Section 4.1

To evaluate the performance of zero-cost proxies in the ImageNet-1K dataset, we compute Spearman's ρ (Krishnakumar et al., 2022b) and Kendall's τ (Ning et al., 2021) rank correlation between the zero-cost proxy scores and the validation accuracy of these sampled networks. We run each experiment over 5 independent runs with different random seeds and compute the mean and standard deviation of rank correlations. As showed by Chen et al. (2021a), the initial weight inherit from the pre-trained supernet can achieve the performance comparable to that of the retrained one, we obtain the true accuracies of sampled network when they inherit their weights from the pre-trained supernet. During the search of ETAS, we first randomly sample 500 networks from the Transformer search space and compute the relative rankings of 500 networks in terms of the zero-cost proxy. After that, we choose the top-3 network structures as the parent population and evaluate these networks to obtain their true performance. For each iteration m, we generate a pool of 100 candidate architectures by mutating the current parent population and select the top-3 architectures from 100 candidate architectures in terms of the zero-cost proxy. The mutation probability is set to 0.4. The parent population is updated by selecting the top-3 networks from the current observed set. We set the number of iterations M to 10. We then find the optimal ViT network from the observed set. At last, we follow the training configuration in AutoFormer Chen et al. (2021a) to train the optimal ViT network and obtain its test accuracy on the test set of ImageNet-1k dataset. All experiments are conducted in a machine with an Intel Xeon Gold 5218R CPU and two NVIDIA GeForce RTX 3090 GPUs.

A.4.2 Experimental settings of Section 4.2

We run each experiment over 5 independent runs with different random seeds and compute the mean and standard deviation of rank correlations. We train each GPT-2 model from scratch following the settings of Radford et al. (2019). Validation perplexity is measured over a sequence length of 192 and 32 tokens for WikiText-103 and LM1B datasets, respectively. We use the BPE tokenizer and set the vocab size to 50264. For the WikiText-103 dataset, we train the GPT-2 network for 4×10^4 steps using the LAMB (You et al., 2020) optimizer with a batch size of 128, a learning rate of 1×10^{-2} with a cosine scheduler, and attention dropout set to 0.1. For the LM1B dataset, we train the GPT-2 network for 1×10^5 steps using the LAMB optimizer with a batch size of 128, a learning rate of 3×10^{-4} with a cosine scheduler, and attention dropout set to 0.1.

During the search of ETAS, we first randomly sample 300 networks from the search space to warm up the entire ETAS algorithm. We compute the relative rankings of these networks in terms of the zero-cost proxy. After that, we choose the top-3 network structures as the parent population and evaluate these networks to obtain their true performance. For each iteration m, we generate a pool of 100 candidate architectures by mutating the current parent population and select the top-3 architectures from the 100 candidate architectures in terms of the zero-cost proxy. The mutation probability is set to 0.3. The parent population is updated by selecting the top-3 networks from the current observed set. We set the number of iterations M to 10. All experiments are conducted on a machine with an Intel Xeon Gold 5218R CPU and two NVIDIA GeForce RTX 3090 GPUs.